Escape from antimicrobial CRISPR-Cas9 in *E. coli* ST131 depends on the genetic context of the target gene.

Running title: *E. coli* ST131 survival of CRISPR-Cas9 antimicrobial.

Clàudia Morros-Bernaus[a#], Joseph Westley[a], Ethan R. Wyrsch[b], Steven P. Djordjevic[b], Lihong Zhang[c], Anne FC. Leonard[c], William H. Gaze[c], David Sünderhauf[a], Stineke van Houte[a#].

[a]Centre for Ecology and Conservation, University of Exeter, Environment and Sustainability Institute, Penryn Campus, TR10 9FE, UK.
[b]Australian Institute for Microbiology and Infection, University of Technology Sydney, Ultimo, NSW 2007, Australia.
[c]European Centre for Environment and Human Health, University of Exeter Medical School, Environment and Sustainability Institute, Penryn Campus, TR10 9FE, UK.

#Correspondence to: c.morros.lab@gmail.com and c.van-houte@exeter.ac.uk.

ABSTRACT

Escherichia coli (*E. coli*) is a common bacterium in the human gut and an important cause of intestinal and extraintestinal infections. Some *E. coli* sequence types (ST) are associated with high pathogenicity. The Extraintestinal Pathogenic *E. coli* (ExPEC) ST131 is a globally distributed multidrug-resistant human pathogen associated with urinary tract and bloodstream infections. Antibiotic-resistant infections often lead to antibiotic treatment failure, underscoring the need of developing alternative treatments. The highly selective antimicrobial potential of CRISPR-Cas9 has been demonstrated in a range of model organisms. However, the effectiveness of CRISPR-Cas9 in combating ST131-associated infections and the consequences of CRISPR-Cas9 treatment, such as the emergence of escapers, remains unclear.

Here, we investigated the antimicrobial activity of CRISPR-Cas9 against ST131 and assessed the frequency and genetic basis of escape. We conjugatively delivered CRISPR-Cas9 to ST131 isolates which carried cefotaxime-resistance-encoding target gene $bla_{CTX\text{-}M\text{-}15}$ in the chromosome and characterized escape subpopulations. Two main types of escapers emerged: $bla_{CTX\text{-}M\text{-}15}$-positive escapers carried dysfunctional CRISPR-Cas9 systems and arose at a ~10^{-5} frequency. Instead, $bla_{CTX\text{-}M\text{-}15}$-negative escapers presented chromosomal deletions involving $bla_{CTX\text{-}M\text{-}15}$ loss. The frequency of $bla_{CTX\text{-}M\text{-}15}$ loss depended on the $bla_{CTX\text{-}M\text{-}15}$ genetic context. Specifically, $bla_{CTX\text{-}M\text{-}15}$-negative escapers emerged at low frequency (~10^{-5}) in isolates where $bla_{CTX\text{-}M\text{-}15}$ was located downstream of insertion sequence (IS) IS*Ecp1*, while escapers emerged with high frequency (~10^{-3}) in isolates where $bla_{CTX\text{-}M\text{-}15}$ was flanked by IS*26*. This work emphasizes how the genetic context of target genes can drive the outcome of CRISPR-Cas9 tools, where the presence of IS*26* may drive increased frequencies of escape.

IMPORTANCE

In the past decade CRISPR-Cas9 has emerged as an efficient antimicrobial tool capable of selective elimination of targeted bacteria. Even though it has been well described that bacteria can evolve to escape targeting by CRISPR-Cas9, the mechanisms of bacterial escape and their consequences remain largely elusive. In this study, we demonstrate the antimicrobial efficacy of CRISPR-Cas9 against natural isolates of *Escherichia coli* ST131, a clinically relevant pathogen, and elucidate the mechanism of escape from antimicrobial activity. We identify two distinct mechanisms of escape, which involve either dysfunctional CRISPR-Cas9 activity, or loss of the target gene ($bla_{\text{CTX-M-15}}$), with the latter occurring at frequencies that depend on the genetic context of the target gene. These findings provide important insights into the frequency and mechanisms of bacterial escape from CRISPR-Cas9-based antimicrobials and offer a foundation for the development of more effective treatments.

Word count abstract: 247

Word count text: 6060

INTRODUCTION

Antimicrobial resistance (AMR) is a global health threat. By 2050, up to 8.22 million annual deaths are predicted to be associated with AMR (1). The misuse and overuse of antibiotics has drastically accelerated the emergence of AMR (2), which contributes to antibiotic treatment failure (3). In this context, *Escherichia coli* is one of the most important pathogens, accounting for the highest number of AMR-attributable deaths in 2019 (4). Therefore, it is recognized by the World Health Organization (WHO) as a priority pathogen for which urgent development of new antimicrobials is needed (5).

Extraintestinal Pathogenic *E. coli* (ExPEC) strains are among the most common Gram-negative pathogens in humans (6). They are associated with numerous types of infections, including urinary tract infections (UTIs), which can develop into bloodstream infections (7–9). Since 2000, Sequence Type (ST) ST131 is the most common pandemic lineage in the clinic (8). The ST131 lineage represents multidrug-resistant pathogens frequently associated with extended-spectrum beta-lactamases (ESBL), aminoglycoside and fluoroquinolone resistance, and several virulence factors (7,9–11). CTX-M enzymes are among the most prevalent type of ESBL (12,13), due to their global dissemination (12,14). The genes encoding these enzymes, $bla_{\text{CTX-M}}$ genes, are found in both chromosomes and plasmids (14,15), often as part of highly mobile genetic structures, surrounded by insertion sequences (IS), transposons and integrons (14). These mobile genetic elements (MGEs) not only contribute to AMR mobilisation but can also act as promoter sequences, regulating expression levels of surrounding genes (14,16,17). Of these, IS are the smallest self-mobilizing units (0.7-2.5 kB) that typically code for a single transposase (Tnp), which allows their mobilisation (18,19). Several families of ISs, notably IS*Ecp1* and IS*26*, are widely distributed across *E. coli* ST131 genomes and are frequently located within or flanking CTX-M gene structures (20–22). While IS*Ecp1* is commonly found as a single copy upstream of the AMR gene (14), IS*26* is often found in multiple copies of the same orientation that flank the AMR gene, in what is known as a pseudo-compound transposon (PCT) (23,24).

ST131-associated infections are difficult to treat. In fact, higher antibiotic treatment failure rates have been reported compared to non-ST131 infections (25,26). In an urgent need to find alternative treatments, CRISPR-Cas9 can be used as a promising novel antimicrobial (27,28). In natural populations, CRISPR-Cas systems act as a prokaryotic immune system against MGE infections. Since its discovery CRISPR-Cas9 in particular has been developed as a highly sequence-specificity tool that can recognize a short (20 bp) specific DNA sequence and subsequently cleave it (29). The tool combines a single-guide RNA (*sgRNA*) with a Cas9 nuclease; the *sgRNA* recognises the target sequence while the Cas9 nuclease executes target cleavage by

81 introducing a blunt-ended double-strand DNA break (DSB) into the target genome (30). DSBs are
82 strong genotoxic lesions that lead to cell death (31). This highly specific antimicrobial effect of
83 CRISPR-Cas9 has been studied extensively over the past ten years (32–36). However, the
84 consequences of CRISPR-Cas9 treatment failure and the long-term effects of its use remain
85 largely unexplored.

86 Here, we assessed the antimicrobial potential of CRISPR-Cas9 targeting *bla*$_{\text{CTX-M-15}}$, the most
87 reported ESBL gene among *E. coli* ST131 (13). We used a modified version of the broad-host range
88 conjugative plasmid pKJK5::csg (37) to deliver CRISPR-Cas9, and programmed CRISPR-Cas9 to
89 target four different *E. coli* ST131 isolates derived from human stool samples (38), all of them
90 carrying a chromosomal copy of *bla*$_{\text{CTX-M-15}}$. While strong antimicrobial activity was observed, we
91 found escapers of CRISPR-Cas9 targeting for all isolates. We observed two main types of
92 escapers, either presenting dysfunctional CRISPR-Cas9, or chromosomal rearrangements
93 leading to loss of the target gene. Interestingly, for the second type of escapers, we found a direct
94 impact of the *bla*$_{\text{CTX-M-15}}$ genetic context (either surrounded by IS*Ecp1* or IS*26*) on the escape
95 frequencies, emphasizing the importance of the genetic context of a target gene on escape from
96 CRISPR-Cas9.

97 **RESULTS**

98 **CRISPR-Cas9 targeting of a chromosomally encoded *bla*$_{CTX-M-15}$ gene in human-associated *E.*
99 *coli* ST131 isolates causes high levels of sequence-specific killing**

100 We used the broad-host range conjugative plasmid pKJK5 as a delivery vector of a CRISPR-Cas9
101 cassette (csgc: *cas9, sgRNA, gfp* and *catB*), either targeting *bla*$_{CTX-M-15}$ (pKJK5::csgc[*bla*$_{CTX-M-15}$]) or a
102 non-targeting control (pKJK5::csgc[NT]). We first verified successful delivery of pKJK5::csgc into
103 a recipient *E. coli* DH5α lacking *bla*$_{CTX-M-15}$, and found no significant differences (p = 0.68) between
104 treatment and control (***Figure 1***), showing that the delivery efficiency of pKJK5::csgc is
105 independent of the *sgRNA* target and that the system can be acquired in the absence of a CRISPR-
106 Cas9 target.

107 Next, we assessed CRISPR-Cas9 targeting activity in four *E. coli* ST131 isolates (Ecp1-I, Ecp1-II,
108 26-I and 26-II); which all carry a single chromosomally encoded *bla*$_{CTX-M-15}$ copy. Completed
109 genome sequences were generated for all four isolates to enable us to have an unambiguous
110 assessment of *bla*$_{CTX-M-15}$ location and copy number. Across isolates, pKJK5::csgc[NT] achieved
111 significantly higher conjugation efficiencies (ranging from 15 ± 8% to 58 ± 11%)) than
112 pKJK5::csgc[*bla*$_{CTX-M-15}$] (ranging from 0.002 ± 0.0007% to 0.062 ± 0.03%; p<0.001) (***Figure 1***). This
113 difference was attributed to the non-viability of transconjugants when CRISPR-Cas9 targets the
114 chromosomally encoded *bla*$_{CTX-M-15}$.

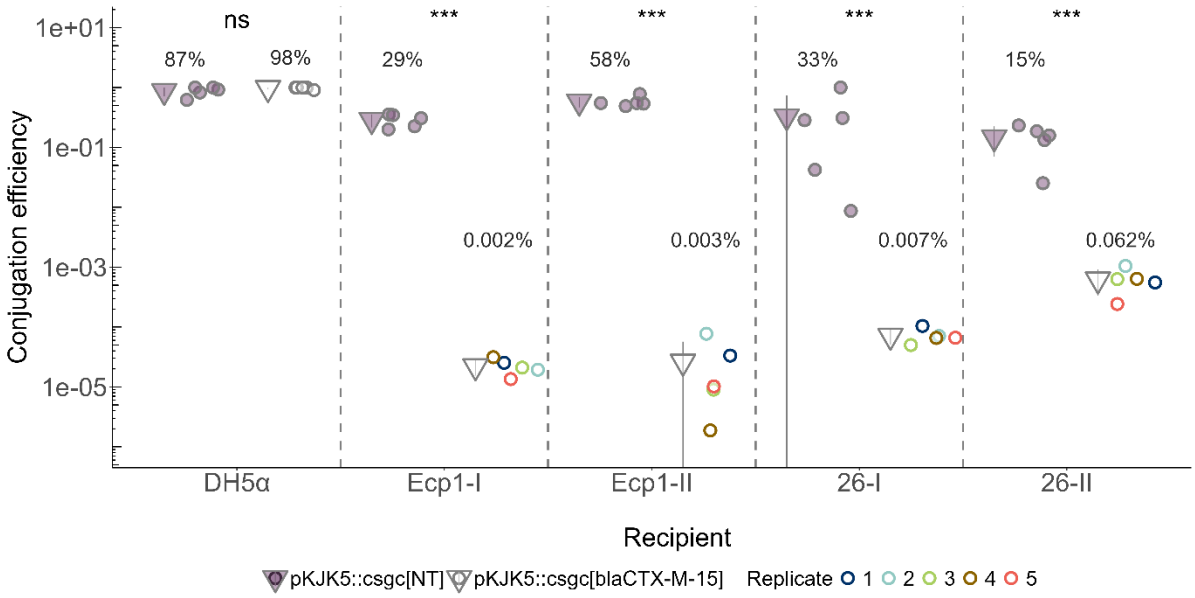

115

116 ***Figure 1:*** Conjugation efficiencies for either pKJK5::csgc[NT] (purple) or pKJK5::csgc[*bla*$_{CTX-M-15}$] (white) across
117 different recipients: either *E. coli* DH5α, lacking *bla*$_{CTX-M-15}$, or the respective *E. coli* ST131 isolates, all with a
118 chromosomally encoded *bla*$_{CTX-M-15}$. Conjugation efficiencies were calculated dividing the number of transconjugants

by the number of recipients. The conjugation efficiencies from the five replicates are represented as circles and the colour represents the replicate number. The distinct colours assigned to each replicate in the pKJK5::csgc[$bla_{CTX-M-15}$] treatment facilitates tracking the replicate origin of the escapers throughout the manuscript. The means of the conjugation efficiencies are represented as triangles ± standard deviation (bars). p-values <0.001 (***), non-significant (ns).

While strong CRISPR-Cas9 antimicrobial activity was demonstrated, all isolates contained subpopulations of *E. coli* ST131 transconjugants (escapers) able to survive acquisition of pKJK5::csgc[$bla_{CTX-M-15}$].

Overall escape frequencies varied across isolates ((4.53 ± 5.30) x 10^{-5} to (4.23 ± 1.95) x 10^{-3}) (***Figure 2A***). To better understand the genetic basis of escape and their relative contribution to the overall escape frequencies, we determined cefotaxime resistance phenotypes for each of the escapers, since resistance to cefotaxime is known to be conferred by CTX-M enzymes (15,39). This showed that both cefotaxime-resistant and cefotaxime-sensitive escapers were found across isolates (***Supplementary figure 3***), revealing that *E. coli* ST131 could escape from CRISPR-Cas9 while either maintaining or losing the target gene.

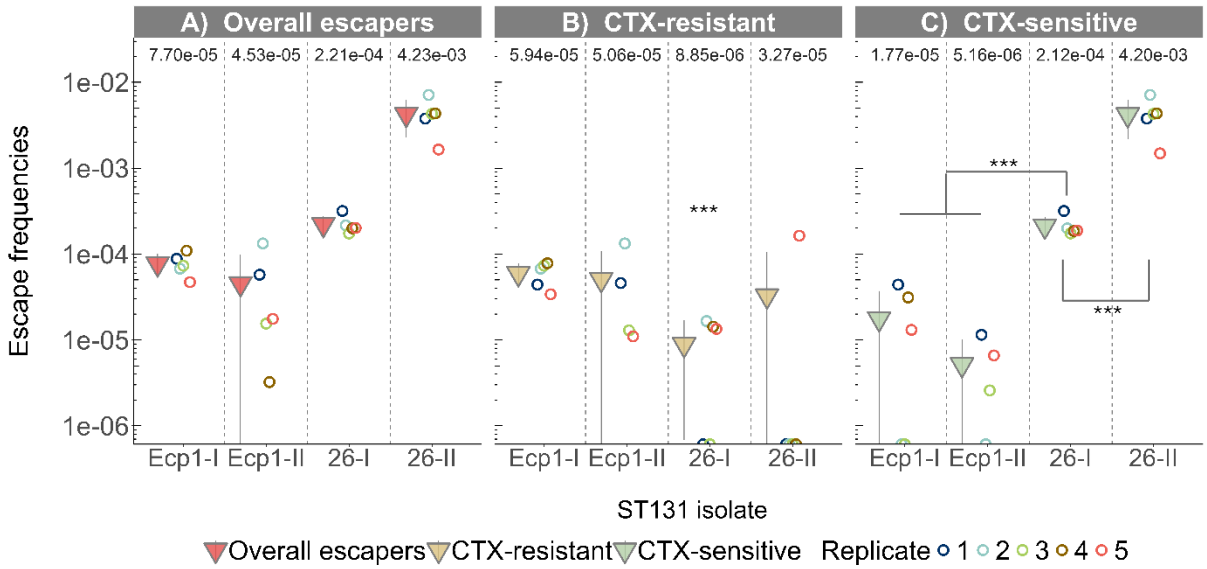

Figure 2: Mean escape frequencies from the CRISPR-Cas9 treatment for the four *E. coli* ST131 isolates. **A**) Overall escape frequencies independent of the cefotaxime resistance phenotype. These frequencies were calculated as the relative conjugation efficiency between the conjugation efficiency of pKJK5::csgc[$bla_{CTX-M-15}$] for each replicate and the average conjugation efficiency of pKJK5::csgc[NT]. **B-C**) Cefotaxime-resistant (**B**) and -sensitive (**C**) escape frequencies. The escape frequencies for each phenotype were determined as the relative conjugation efficiency between the cefotaxime-resistant or cefotaxime-sensitive conjugation efficiencies of pKJK5::csgc[$bla_{CTX-M-15}$] for each replicate and the average conjugation efficiency of pKJK5::csgc[NT]. The escape frequencies from the five replicates are represented as circles and the colour represents the replicate number. The mean escape frequencies, which include replicates with no escapers for a specific phenotype, are represented as triangles ± standard deviation (bars). Replicate 4 from isolate Ecp1-II was excluded from cefotaxime-resistant and cefotaxime-sensitive escape frequencies as only one escaper could be directly recovered from the filter mating assay. p-values <0.001 (***).

<u>Cefotaxime-resistant escapers have dysfunctional CRISPR-Cas9 systems.</u>

147 Cefotaxime-resistant escape frequencies were generally low (~10^{-5}) but showed significant
148 variation across isolates (***Figure 2B*****;** $p<0.001$). Post-hoc testing revealed this was due to isolate
149 26-I having a significantly lower escape frequency than all others ($p<0.001$). Nevertheless, the
150 escape frequencies for isolates 26-I and 26-II should be interpreted cautiously, as only few
151 escapers were detected, and their presence was inconsistent across replicates (***Figure 2B*** and
152 ***Supplementary figure 3***). Therefore, in-depth analysis of cefotaxime-resistant escapers was
153 only performed for isolates Ecp1-I and Ecp1-II. First, we sequenced the $bla_{CTX\text{-}M\text{-}15}$ gene to
154 genetically confirm the cefotaxime-resistant phenotypes and found no mutations in the target
155 site or PAM. We then hypothesized that escapers likely survived CRISPR-Cas9 targeting through
156 acquiring mutations in *cas9* and/or *sgRNA* (csgc) on the pKJK5::csgc[$bla_{CTX\text{-}M\text{-}15}$]. To address this,
157 we assessed CRISPR-Cas9 integrity using PCR. All transconjugants from the pKJK5::csgc[NT]
158 control showed expected $bla_{CTX\text{-}M\text{-}15}$ and csgc amplicons, but deletions, duplications, and partial
159 or complete lack of amplification within *cas9* and/or *sgRNA* were found for 48% (Ecp1-I) and 64%
160 (Ecp1-II) of the escapers (***Supplementary figure 4A***). Furthermore, one Ecp1-II escaper exhibited
161 an IS150 transposition into *cas9*. While IS150 is present in both the donor (K-12 MG1655) and the
162 recipient (ST131 isolate Ecp1-II) genome, the presence of a single nucleotide polymorphism
163 unique for IS150 in the K-12 genome suggested that the transposition into pKJK5::csg[$bla_{CTX\text{-}M\text{-}15}$]
164 occurred in the donor prior to its delivery to Ecp1-II. The different mutations were distributed
165 across the *cas9* and *sgRNA* sequence (***Supplementary figure 4B-C***), with no obvious patterns
166 revealed except for a hotspot in the α-helical lobe found in escapers from isolate Ecp1-I
167 (***Supplementary figure 4B***) (40).

168 Those escapers that did not exhibit identifiable csgc mutations were subjected to a phenotypic
169 CRISPR-Cas9 functionality assay. We mated escapers with a donor bacterium bearing either
170 targeted plasmid pCTX15 (carrying the wildtype $bla_{CTX\text{-}M\text{-}15}$) or untargeted plasmid pCTRL
171 (***Supplementary figure 5A***) and calculated their relative conjugation efficiencies
172 (pCTRL/pCTX15). Cefotaxime-sensitive escapers lacking $bla_{CTX\text{-}M\text{-}15}$ were used as potential
173 positive CRISPR-Cas9 controls. For both Ecp1-I and Ecp1-II most cefotaxime-sensitive escapers
174 demonstrated protection against pCTX15 (***Supplementary figure 5B-C***). In contrast, no
175 protection was observed for cefotaxime-resistant escapers (***Supplementary figure 5B-C***),
176 indicating dysfunctional CRISPR-Cas9 activity. Only one cefotaxime-resistant escaper (5.10
177 Ecp1-II) showed a relative conjugation efficiency for all the replicates compatible with functional
178 CRISPR-Cas9 activity (***Supplementary figure 5C***), which could indicate coexistence of the
179 wildtype $bla_{CTX\text{-}M\text{-}15}$ and a functional pKJK5::csgc[$bla_{CTX\text{-}M\text{-}15}$]. This escaper showed no mutations in
180 $bla_{CTX\text{-}M\text{-}15}$, and short-read WGS did not reveal relevant mutations in pKJK5::csgc[$bla_{CTX\text{-}M\text{-}15}$] that

181 could interfere with CRISPR-Cas9 activity. Therefore, coexistence could be attributed to an
182 unknown mechanism.

183 To summarize, we found that cefotaxime-resistant escape frequencies were ~10^{-5} across isolates
184 and all the escapers carried *bla*$_{\text{CTX-M-15}}$ with no mutations in the protospacer or PAM sequence.
185 Using genotypic and phenotypic screening, we attributed cell survival to dysfunctional CRISPR-
186 Cas9 systems.

187 **Cefotaxime-sensitive escapers lost *bla*$_{\text{CTX-M-15}}$ in a manner dependent on its genetic**
188 **context.**

189 To understand the differential cefotaxime-sensitive escape frequencies found across isolates
190 (***Figure 2C***), we sought to understand the genetic context of *bla*$_{\text{CTX-M-15}}$. Long-read genome
191 analyses of the ancestral untreated isolates revealed three different genetic contexts. In isolates
192 Ecp1-I and Ecp1-II, *bla*$_{\text{CTX-M-15}}$ is found downstream of an insertion sequence (IS) IS*Ecp1*, which
193 disrupts *lacY* in the *lac* operon (***Figure 3A***). In contrast, isolates 26-I and 26-II carry *bla*$_{\text{CTX-M-15}}$
194 flanked by two IS*26* copies of the same orientation, in a pseudo-compound transposon (PCT)
195 (18,23). This *bla*$_{\text{CTX-M-15}}$ PCT is found surrounded by either two or three additional IS*26* copies
196 respectively, creating two slightly distinct overall IS*26*-contained sequences. These sequences
197 share the same genome location in both isolates, disrupting a gene of unknown function
198 (*EC958_2451*) (***Figure 3B-C***). Significant differences were found between cefotaxime-sensitive
199 escape frequencies of the three genetic contexts (p-values for each combination < 0.001).
200 Isolates with an IS*Ecp1* genetic context showed significantly lower cefotaxime-sensitive escape
201 frequencies than isolate 26-I (4-copy IS*26* context), which in turn had a significantly lower escape
202 frequency than isolate 26-II (5-copy IS*26* context). Overall, this indicates a significantly higher
203 escape frequency through loss of *bla*$_{\text{CTX-M-15}}$ in isolates with an IS*26* genetic context compared to
204 IS*Ecp1*. Consequently, different approaches were employed to characterize the escapers based
205 on their genetic context.

206

207

208

209

210

211

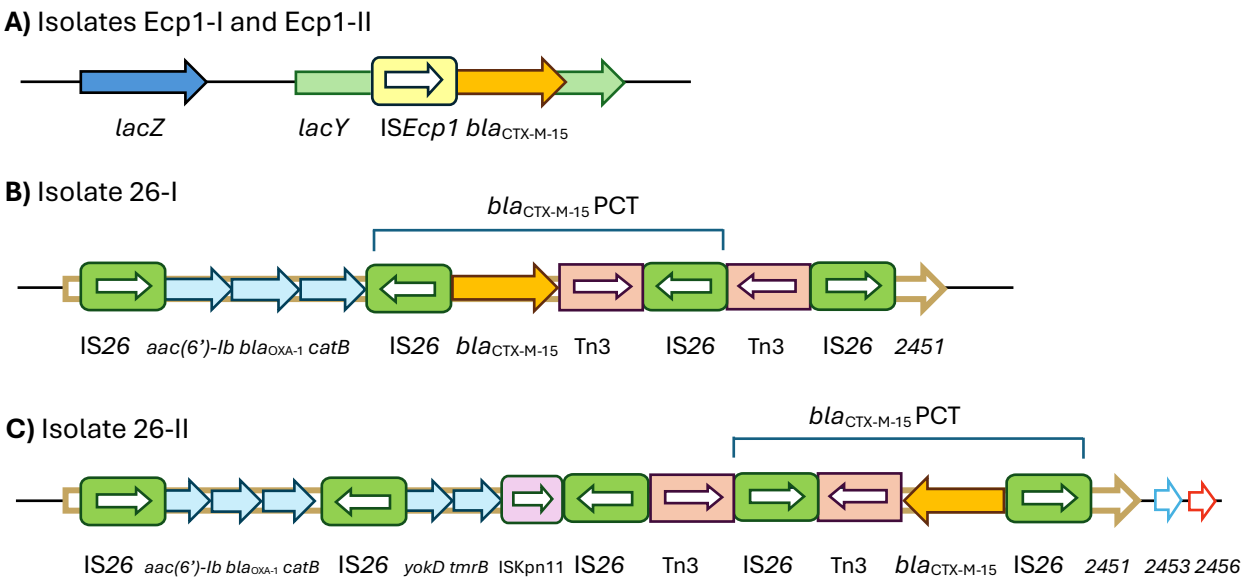

Figure 3: Genetic context of *bla*$_{CTX-M-15}$ (orange arrow) for the four *E. coli* ST131 isolates, ORFs and gene distances not drawn to scale. **A**) Isolate Ecp1-I and Ecp1-II share the same ISEcp1 genetic context disrupting a *lacY* gene. The *lacZ* gene is found 1.2 kB upstream of the IS*Ecp1*. IS*Ecp1* is represented as a yellow arrow box. **B-C**) IS*26* genetic contexts for isolates 26-I (**B**) and 26-II (**C**), with a *bla*$_{CTX-M-15}$ pseudo-compound transposon (PCT). For both isolates, the respective overall IS*26*-contained sequences are found disrupting the gene with unknow function (*EC958_2451*), shown in the figure as 2451. The two Tn3, shown as pink boxes, represent a single Tn3 split into two truncated ORFs, likely due to IS*26* disruption that led to an inversion of one of the parts. IS*26* is represented as a green arrow box. *2453* and *2456* represent the genes *EC958_2453 and EC958_2456*.

An IS*Ecp1* genetic context is associated with large-scale genomic deletions alongside *bla*$_{CTX-M-15}$ loss.

For cefotaxime-sensitive escapers from Ecp1-I (n=19) and Ecp1-II (n=19) (***Supplementary figure 3***), PCR and subsequent Sanger sequencing of the amplicons revealed complete loss of IS*Ecp1* + *bla*$_{CTX-M-15}$ for most of the escapers (n=36) and partial deletions including the protospacer sequence (the 20 bp targeted by pKJK5::csgc[*bla*$_{CTX-M-15}$]) for the remaining escapers (n=2) (***Supplementary figure 6A***).

To better characterize the dimensions of the IS*Ecp1* + *bla*$_{CTX-M-15}$ deletions, a β-galactosidase assay was performed, taking advantage of the proximal *lacZ* gene (***Figure 3A***). This enzymatic assay allows phenotypic screening of blue or white colonies based on presence or absence, respectively, of β-galactosidase, the enzyme encoded by *lacZ*. A negative phenotype (white) indicated deletions of IS*Ecp1* + *bla*$_{CTX-M-15}$ together with *lacZ* (***Supplementary figure 6B***). In contrast, a positive phenotype (blue) delimited the start of the deletion within 1.2 kB (somewhere in between *lacZ* and IS*Ecp1*) (***Supplementary figure 6C***). Both phenotypes were observed across escapers, with β-galactosidase-negative escapers being more abundant (n=30) (***Supplementary***

236 ***figure 6D***). Short-read WGS was performed on a representative escaper from each phenotype
237 and isolate to confirm their genotypic basis.

238 Additionally, all cefotaxime-sensitive escapers from Ecp1-I and Ecp1-II were subjected to both
239 the csgc genotypic and phenotypic CRISPR-Cas9 functionality assay previously described. All
240 escapers showed csgc amplicons of expected lengths. In the phenotypic assay most showed
241 functional CRISPR-Cas9 systems (n=32). Nevertheless, a small subset showed dysfunctional
242 CRISPR-Cas9 activity (n=6), highlighting that both the loss of $bla_{\text{CTX-M-15}}$ and the presence of a
243 dysfunctional system can co-occur (***Supplementary figure 5B-C***).

244 **An IS*26* genetic context is associated with small-scale genomic deletions of $bla_{\text{CTX-M-15}}$**
245 **facilitated by the presence of two flanking IS*26* copies.**

246 For isolates 26-I and 26-II, both with an IS*26* genetic context, 26-II was chosen as a representative
247 for further study due to its higher IS*26* load (***Figure 3 B-C***). First, hybrid WGS was performed for a
248 subset of escapers (n=10) which revealed either the deletion of the $bla_{\text{CTX-M-15}}$ PCT (n=8) or larger
249 deletions including downstream chromosomal sequences (n=2). All the deletions led to a single
250 remaining IS*26* chromosomal copy from the two original ones.

251 We used these representative data to inform PCRs assaying the deletion of the $bla_{\text{CTX-M-15}}$ PCT
252 (***Supplementary figure 7A***) in all the cefotaxime-sensitive escapers (n=98). The ancestral isolate
253 and the cefotaxime-resistant escapers (used as positive controls) showed the expected 4.9 kB
254 amplicon covering the $bla_{\text{CTX-M-15}}$ PCT alongside a smaller amplicon, likely a PCR artefact resulting
255 from recombination between the multiple copies of IS*26*. Crucially, cefotaxime-sensitive
256 escapers (n=94) lacked the 4.9 kB amplicon and only displayed a 972 bp amplicon, which
257 corresponded to a single IS*26* copy in agreement with the deletion of the $bla_{\text{CTX-M-15}}$ PCT observed
258 in the WGS (***Supplementary figure 7B***). Additionally, 3 escapers, including the two with larger
259 deletions characterized by WGS, showed no amplicon, agreeing with the presence of larger
260 deletions thus avoiding primer binding (***Supplementary figure 7A and C-D***). Finally, one escaper
261 showed a <4.9 kb amplicon, likely explained by a partial deletion within $bla_{\text{CTX-M-15}}$, thereby
262 conferring loss of the resistant phenotype and escape of CRISPR-Cas9 targeting.

263 To summarize, the emergence of cefotaxime-sensitive escapers was significantly impacted by
264 the genetic context of $bla_{\text{CTX-M-15}}$. While all cefotaxime-sensitive escapers exhibited chromosomal
265 rearrangements involving the loss of $bla_{\text{CTX-M-15}}$, an IS*Ecp1* genetic context was associated with
266 lower escape frequencies and large-scale deletions. In contrast, an IS*26* genetic context revealed

267 higher escape frequencies, primarily driven by small-scale deletions (*bla*$_{CTX-M-15}$ PCT) occurring
268 between the two flanking IS*26* elements.

269 **DISCUSSION**

270 Here, we demonstrated the sequence-specific antimicrobial activity of CRISPR-Cas9 by targeting
271 the chromosomally encoded ESBL gene *bla*$_{CTX-M-15}$ in human-associated isolates of the *E. coli*
272 lineage ST131. The delivery of a *bla*$_{CTX-M-15}$ targeting CRISPR-Cas9 cassette using the broad host-
273 range conjugative plasmid pKJK5::csgc achieved a significant reduction (from 236-fold to 22.000-
274 fold, depending on the isolate) in conjugation efficiency compared to a non-targeting control,
275 explained by the non-viability of *E. coli* ST131 transconjugants. This demonstrates the
276 antimicrobial use of CRISPR-Cas9 against *E. coli* ST131 isolates, which can be found in
277 antimicrobial resistant UTIs, for which non-antibiotic treatments are urgently needed (41).
278 Promisingly, the use of pKJK5::csgc is compatible with probiotics, which are already prophylactic
279 and therapeutic treatment options for recurrent UTIs (42–44). However, we observed widespread
280 escape of CRISPR-Cas9 targeting across isolates and identified both escapers that retained the
281 *bla*$_{CTX-M-15}$ gene and carried dysfunctional CRISPR-Cas9, and escapers that lost *bla*$_{CTX-M-15}$ through
282 chromosomal rearrangements. Crucially, for the escapers with *bla*$_{CTX-M-15}$ deletions, we found
283 significantly different escape frequencies depending on the genetic context of the target gene,
284 with increased escape frequencies (up to 813-fold) when *bla*$_{CTX-M-15}$ is found surrounded by two
285 copies of IS*26*, as part of an IS*26* pseudo-compound transposon (PCT), compared to when it is
286 found downstream of an IS*Ecp1*.

287 Cefotaxime-resistant (*bla*$_{CTX-M-15}$-positive) escapers retained an intact version of *bla*$_{CTX-M-15}$,
288 suggesting that CRISPR-Cas9 escape through mutations in the protospacer (the 20 bp targeted
289 by pKJK5::csgc[*bla*$_{CTX-M-15}$]) or protospacer adjacent motif (PAM) sequence is rare in these isolates.
290 As mutations in the target site were previously reported for other genes (36,45–49), we
291 hypothesize that the absence of such escapers in our setup may be attributed to mutations in
292 *bla*$_{CTX-M-15}$ occurring below the detection limit of the assay (~10^{-6}). Instead, all cefotaxime-resistant
293 escapers presented dysfunctional CRISPR-Cas9 systems. In line with previous literature
294 (35,45,46,48,50,51), we found deletions, duplications and insertions across *cas9* and *sgRNA*.
295 Interestingly, we only found one escaper with an IS transposition into *cas9*, even though this is a
296 commonly reported event (36,46,47,50,52). To minimize escapers with dysfunctional CRISPR-
297 Cas9 systems, several solutions have been proposed, including the use of multi-target arrays
298 (35,36,48), the manipulation of the CRISPR-Cas9 plasmid copy number (50), coupling CRISPR-
299 Cas antimicrobials with CRISPR-regulated toxin-antitoxin systems (ATTACK) (53) or the use of

300 non-DNA based delivery strategies such as nano-sized CRISPR complexes (54), especially as
301 plasmid-based delivery relies on often heterogenous transcriptional activity of recipients (55).
302 However, the optimal solution to this problem has yet to be established.

303 In contrast, cefotaxime-sensitive escapers revealed *bla*$_{CTX-M-15}$ deletions, and this loss of the target
304 gene occurred in significantly higher frequencies (up to 813-fold) for isolates with an IS*26* genetic
305 context compared to an IS*Ecp1* genetic context. The observed *bla*$_{CTX-M-15}$ deletions were likely
306 driven by homologous recombination (HR), which could either occur in the pre-existing
307 population leading to positively selected genotypes upon CRISPR-Cas9 exposure, or as a DNA-
308 damage repair mechanism after CRISPR-Cas9 targeting and a subsequent triggering of the SOS
309 response (33,36,56). Escapers with successful DNA-damage repair could be associated with
310 weaker CRISPR-Cas9 activity (33), poor *sgRNA* folding (57) or expression (58) and/or variability in
311 the host DNA damage tolerance and responses (59). Deletions of *bla*$_{CTX-M-15}$ compatible with HR
312 were observed across isolates. For isolates Ecp1-I and Ecp1-II, sequencing of few cefotaxime-
313 sensitive escapers revealed deletions with border homology (9-11 bp), likely indicating HR. In
314 isolate 26-II, the most common deletion observed among cefotaxime-sensitive escapers (a
315 deletion of the *bla*$_{CTX-M-15}$ PCT leaving a single IS*26* copy in the chromosome; ***Supplementary***
316 ***figure 7B***), is consistent with the product of HR between the two directly oriented IS*26* copies
317 (60–62) (***Supplementary figure 8A-B***). Recombination before CRISPR-Cas9 cleavage would
318 release a circular molecule carrying *bla*$_{CTX-M-15}$, known as a translocatable unit (TU)
319 (18,24,60,63,64), (***Supplementary figure 8A***) which is expected to be readily lost in absence of
320 self-replicative features (60) or through active targeting by CRISPR-Cas9. CRISPR-Cas9 cleavage
321 of intermediate circular molecules from similar excised MGEs has been recently reported (65).
322 Overall, the higher escape frequencies observed in an IS*26* genetic context could be attributed to
323 the homology found between the several IS*26* copies (***Figure 3 B-C***), which may facilitate HR. In
324 fact, HR between homologous IS elements is a common driver of chromosomal rearrangements
325 in *E. coli* (66).

326 Alternatively, *bla*$_{CTX-M-15}$ loss could be driven by an incomplete IS-mediated *bla*$_{CTX-M-15}$ mobilization.
327 Evidence of this was found in escapers from isolate 26-II with larger *bla*$_{CTX-M-15}$ deletions lacking
328 homology in the borders (***Supplementary figure 7C-D***). These deletions likely resulted from a
329 Tnp26-dependent intramolecular copy-in mobilisation (24,67), in where the downstream genes
330 *EC958_2453* and *EC958_2456* would have been used as respective intramolecular targets to
331 mediate chromosomal excision, releasing a TU carrying the enclosed sequence (60)
332 (***Supplementary figure 8CI-II***), which would be readily lost or targeted by CRISPR-Cas9. This
333 mobilization pattern could also contribute to escapers with a *bla*$_{CTX-M-15}$ PCT deletion, if using the

334 sequence found downstream of the PCT as an intramolecular target site (***Supplementary figure***
335 ***8CIII***). In contrast, we could not find evidence of *bla*$_{CTX-M-15}$ deletions mediated by IS*Ecp1*
336 mobilisation, as IS*Ecp1* mobilises together with downstream genes (18,68–71). Therefore, this
337 would only be possible in *lacZ*-positive cefotaxime-sensitive escapers, which are a minority
338 (***Supplementary figure 6D***). Sequencing of two *lacZ*-positive escapers revealed *bla*$_{CTX-M-15}$
339 deletions incompatible with IS*Ecp1* mobilisation, suggesting that this is not a common escape
340 mechanism.

341 To summarize, even though our data does not allow us to discern the exact escape mechanism
342 that leads to chromosomal rearrangements, deletions resulting from both HR and incomplete IS-
343 mediated *bla*$_{CTX-M-15}$ mobilization are not mutually exclusive, and it is likely that the total escape
344 population is a combinatorial result of these events, each occurring at different frequencies.

345 Escapers with chromosomal rearrangements involving the deletion of the target gene have been
346 reported for other genes and bacterial species (33,36,49,57,72–74), including deletions with
347 border homology, suggesting HR (33,75,76). Additionally, some studies have shown a reduction
348 in escape frequencies when knocking out (33) or inhibiting (57) expression of RecA, an important
349 protein involved in HR (77) and found in all the ST131 isolates used in this work. Interestingly,
350 studies where the target gene is found within a chromosomally integrated MGE reported escapers
351 in which the entire MGE was deleted, similar to the deletions of the *bla*$_{CTX-M-15}$ PCT reported here.
352 This occurred when the target genes were in a genomic island flanked by two directly oriented
353 IS1193 copies (73), in several pathogenicity islands (49,78) and in prophages (78).

354 The presence of escapers with chromosomal rearrangements after a CRISPR-Cas9 treatment
355 might be especially relevant when occurring at high frequencies, as for isolate 26-II (~10^{-3}). The
356 emergence of this type of escapers could likely be reduced by choosing target genes independent
357 from chromosomally integrated MGEs and with genetic contexts that present limited or no
358 homology. In this study, escapers with *bla*$_{CTX-M-15}$ loss were resensitized to cefotaxime, which
359 could be a beneficial outcome for antibiotic therapy. However, this type of chromosomal
360 rearrangements can also involve loss of other genes, leading to phenotypic changes (73,76).
361 Furthermore, deletions resulting from successful DNA repair after CRISPR-Cas9 cleavage
362 through HR could be accompanied by mobilisation of other HR-mediated MGEs (18). This might
363 be especially relevant when using CRISPR-Cas9 against AMR-carrying bacteria, which often carry
364 MGEs (18). While we did not directly observe this, such far-reaching genomic consequences of
365 CRISPR-Cas9 targeting should also be kept in mind when using CRISPR-Cas9 as an editing tool,
366 which often relies on HR (31,58).

367 Altogether, this study showed the antimicrobial activity of CRISPR-Cas9 against the
368 chromosomally encoded AMR gene *bla*$_{CTX-M-15}$ from human-associated *E. coli* ST131 isolates and
369 identified escapers resulting from either dysfunctional CRISPR-Cas9 or with chromosomal
370 rearrangements that led to the deletion of *bla*$_{CTX-M-15}$. Our work showed the impact that the genetic
371 context of the target gene has on escape frequencies, where an association with IS*26* led to a high
372 frequency of *bla*$_{CTX-M-15}$ loss. This research underlines the importance of understanding the genetic
373 environment to be able to predict the treatment outcome of CRISPR-Cas9 antimicrobials and
374 CRISPR-Cas9 gene editing. Finally, we also want to highlight the potential use of CRISPR-Cas9 as
375 a tool to better characterize IS mobilization patterns by studying escapers arising from the
376 targeting of the IS elements or cargo genes.

377 **METHODS**

378 **Growth conditions, buffers and media**

379 Lysogeny broth (LB), either liquid or mixed with agar, was used as growth media. Antibiotics were
380 used to ensure plasmid maintenance, select for chromosomal markers or perform phenotypic
381 assays at: chloramphenicol (Cm) 25 µg mL^{-1}, gentamicin (Gm), kanamycin (Km) and streptomycin
382 (Sm) all 50 µg mL^{-1}, and cefotaxime (CTX) 5 µg mL^{-1}. Glycerol stocks were prepared at 20% (w/v)
383 and frozen at -70 °C. Sterile 0.9 % (w/v) NaCl was used as a buffer as indicated. Unless otherwise
384 specified, all kits and reagents were used following manufacturer's instructions and incubations
385 were performed overnight (O/N) at 37 °C, 180 rpm.

386 **Bacterial strains**

387 We selected the *E. coli* ST131 isolates used in this study (Ecp1-I, Ecp1-II, 26-I and 26-II) based on
388 the genetic context of *bla*$_{CTX-M-15}$ (genomes deposited on Genbank under BioProject
389 PRJNA1281408). All the ST131 isolates belong to clade C, the most relevant in the clinic (79).
390 Isolates Ecp1-I, Ecp1-II and 26-I were chromosomally tagged with an *aacC1* gene, conferring Gm
391 resistance, through electroporation of a Tn5 transposon plasmid pBAMD1-6 (80), followed by PCR
392 screening to confirm absence of residual plasmid as well as competition experiments against the
393 respective ancestral isolates to verify that tagging did not incur a fitness cost. In brief, the
394 modified strains were grown together with their wildtype variants, and colony counts revealed
395 similar growth. Isolate 26-II was not genetically modified due to intrinsic Gm resistance. *E. coli* K-
396 12 MG1655::*mCherry* (81) was used as CRISPR-Cas9 donor strain because it represses
397 expression of *gfp* from pKJK5::csgc, which allows us to verify successful plasmid conjugation to

398 the ST131 isolates (presence of transconjugants) by checking *gfp* expression. Further bacteria
399 and plasmid information can be found in ***Supplementary table 1*** and ***2***, respectively.

400 **Development of the CRISPR-Cas9 system**

401 Two CRISPR-Cas9 cassettes were designed with distinct *sgRNA* targets. The [$bla_{CTX\text{-}M\text{-}15}$] *sgRNA*
402 targets [CGCGTGATACCACTTCACCT]. This sequence is found within $bla_{CTX\text{-}M\text{-}15}$ and followed by a
403 protospacer adjacent motif (PAM) in the *E. coli* ST131 reference genome (82) and the genome of
404 the four *E. coli* ST131 isolates used in the study. Furthermore, the sequence showed low
405 predicted CRISPR-off target activity in both CRISPOR (83) and Cas-OFFinder (84). The non-
406 targeting [NT] control *sgRNA* targets random nucleotide sequence [GGTAAGACCATTAGAAGTAG],
407 20 bp which we confirmed to be absent from all *E. coli* ST131 isolates. These cassettes were
408 generated and transferred into pKJK5, resulting in pKJK5::csgc[$bla_{CTX\text{-}M\text{-}15}$] or [NT], following
409 protocols adopted from (37) (full details in ***Supplementary method 1*** and ***Supplementary table***
410 ***3***).

411 **Filter mating conjugation *E. coli* K-12 MG1655 (donor) - *E. coli* ST131 (recipient)**

412 Single colonies of donors (MG1655 pKJK5::csgc[$bla_{CTX\text{-}M\text{-}15}$] or [NT]) and recipients (*E. coli*
413 DH5α::SmR or the respective *E. coli* ST131 isolates) were grown O/N in 5 mL LB. Donors were
414 supplemented with Cm to avoid segregational loss of pKJK5. Cells were washed twice in 5 mL
415 NaCl, followed by OD600 adjustment to 0.5 – 0.6. Recipients were diluted 100-fold in NaCl. Filter
416 mating was performed in a Millipore 1225 Sampling Manifold using a sterile Whatman Cyclopore
417 Clear 0.2 µm 25mm polycarbonate membrane on top of a sterile Whatman glass microfiber filter,
418 binder free, grade GF/C, 25mm. The vacuum manifold was sterilised using ethanol and UV before
419 and between batches. Filters were washed by pumping through 2 mL of NaCl. Straight after, 1 mL
420 of NaCl, 1 mL of donor and 1 mL of a 100-fold diluted recipient were pumped through. Five
421 biological replicates were performed for each donor-recipient combination. Additionally,
422 controls with donor-only, recipient-only and NaCl-only were performed and yielded results
423 consistent with expectations, supporting the validity of the experiment. The polycarbonate filters
424 were placed onto 10 % LB-agar plates and incubated for 48 h at 37 °C in the absence of
425 antibiotics. Filters were recovered in 3 mL NaCl and vortexed. From the cell suspension, cells
426 were recovered in LB, after which differential selective plating on LB agar was used to quantify
427 the proportion of 1) donors (no antibiotic selection; donors identified by assessing *mCherry*
428 expression using a stereo fluorescent lamp (Nightsea), 2) recipients (Gm) and 3) transconjugants
429 (Gm + Cm). Glycerol stocks were made with the remaining cell suspensions.

430 For each replicate, conjugation efficiency was calculated by dividing transconjugant
431 concentrations (CFU/mL) by recipient concentrations (CFU/mL) and means were determined for
432 each isolate and treatment. For each replicate from the pKJK5::csgc[$bla_{CTX\text{-}M\text{-}15}$] treatment, escape
433 frequencies were calculated as a relative conjugation efficiency by dividing the conjugation
434 efficiency of pKJK5::csgc[$bla_{CTX\text{-}M\text{-}15}$] for each replicate with the average conjugation efficiency of
435 pKJK5::csgc[NT]. The mean escape frequency per isolate was calculated as the average of all five
436 biological replicates.

437 **Recovery of *E. coli* ST131 escapers (*E. coli* ST131 pKJK5::csgc[$bla_{CTX\text{-}M\text{-}15}$]) and phenotypic**
438 **analysis**

439 *E. coli* ST131 pKJK5::csgc[$bla_{CTX\text{-}M\text{-}15}$] escapers were recovered on Gm + Cm plates and the
440 presence of $bla_{CTX\text{-}M\text{-}15}$ was verified based on their cefotaxime resistance profile. To do so,
441 individual clones were replated onto LB agar containing (i) Cm + CTX and (ii) Cm to assess the
442 cefotaxime phenotype while ensuring CRISPR-Cas9 plasmid maintenance. Additionally, we
443 generated glycerol stocks of escapers after O/N incubation in LB + Cm. The same procedure was
444 used to select for 100 transconjugants from the non-targeting treatment (*E. coli* ST131
445 pKJK5::csgc[NT]). A visual representation of the filter mating assay and the phenotypic screen of
446 the escapers can be found in ***Supplementary figure 1*.**

447 To calculate cefotaxime-resistant and cefotaxime-sensitive escape frequencies, the cefotaxime
448 resistance profiles were assessed for all escapers recovered directly from the filter mating assay
449 for isolates Ecp1-I, Ecp1-II and 26-I. For isolate 26-II, due to the larger size of the escape
450 population recovered, ten escapers per replicate were randomly selected for resistance profiling.
451 The proportions of each cefotaxime phenotype were then used to estimate cefotaxime-resistant
452 and cefotaxime-sensitive transconjugants concentrations (CFU/mL) per replicate. Conjugation
453 efficiencies for both phenotypes were calculated by dividing the respective transconjugant
454 concentrations by the recipient concentrations for each replicate of the pKJK5::csgc[$bla_{CTX\text{-}M\text{-}15}$]
455 treatment. Finally, cefotaxime-resistant and cefotaxime-sensitive escape frequencies were
456 calculated as a relative conjugation efficiency by dividing the cefotaxime-resistant or cefotaxime-
457 sensitive conjugation efficiencies of pKJK5::csgc[$bla_{CTX\text{-}M\text{-}15}$] for each replicate with the average
458 conjugation efficiency of pKJK5::csgc[NT]. The mean escape frequency per phenotype and
459 isolate was calculated as the average of all biological replicates, including those where no
460 cefotaxime-resistant or cefotaxime-sensitive escapers were found. Replicate 4 from isolate
461 Ecp1-II was excluded from the calculations of cefotaxime-resistant and cefotaxime-sensitive
462 escape frequencies as only one escaper was directly recovered from the filter mating assay.

463 **Genotypic analysis of *bla*$_{CTX-M-15}$**

464 PCR was used to study *bla*$_{CTX-M-15}$ presence in escapers. To obtain enough DNA template material,
465 frozen glycerol stocks of escapers were scraped with a pipette tip and the tip was swirled in 10 µL
466 water to suspend attached material. The suspension was then heated to 95 °C for 15 minutes and
467 centrifugated at 3.500 rpm for 5 minutes. For cefotaxime-resistant and cefotaxime-sensitive
468 escapers from isolates Ecp1-I and Ecp1-II, *bla*$_{CTX-M-15}$ presence was studied using primers with
469 binding sites within the gene (***Supplementary figure 2A***). Furthermore, for the cefotaxime-
470 sensitive escapers primers designed to amplify IS*Ecp1* + *bla*$_{CTX-M-15}$ were also used
471 (***Supplementary figure 2A***). Phusion High-Fidelity polymerase (Thermo Scientific) was used in
472 both PCRs. Additionally, ExoSAP-cleaned (NEB) PCR amplicons were Sanger sequenced. In
473 cefotaxime-sensitive escapers from isolate 26-II, the deletion of the *bla*$_{CTX-M-15}$ PCT was studied
474 using primers annealing outside the PCT (***Supplementary figure 2B***) with 1x VeriFi Hot Start
475 Polymerase (PCR Biosystems). Across PCRs, when no amplicon was found, 16S PCR or
476 amplification of other genes were used to verify template presence. Moreover, the respective
477 ancestral isolates and transconjugants from the non-targeting control (pKJK5::csgc[NT]) were
478 used as positive controls for the presence of *bla*$_{CTX-M-15}$. All primers can be found in
479 ***Supplementary table 3***.

480 **Genotypic analysis of CRISPR-Cas9 integrity**

481 Cefotaxime-resistant and cefotaxime-sensitive escapers from isolates Ecp1-I and Ecp1-II were
482 subjected to a genotypic CRISPR-Cas9 integrity assay to understand whether mutations had
483 occurred in *cas9* and/or the *sgRNA*. Four sets of primers generating overlapping amplicons were
484 used, including a region upstream of *cas9* and downstream of the *sgRNA*. Additionally, a fifth set
485 was used to specifically amplify the *sgRNA* (***Supplementary figure 2C***). PCRs were performed
486 using 2x PCRBIO Taq Mix Red (PCR Biosystems). Amplicons with unexpected lengths (i.e.
487 amplicons with an estimated length >60 bp different from the expected amplicon length) were
488 purified from the agarose gel using the Monarch® DNA Gel Extraction Kit Protocol (NEB) and
489 Sanger sequenced. Transconjugants from the pKJK5::csgc[NT] control and the ancestral isolates
490 were used as controls, and 16S amplification was used to verify template presence. DNA
491 template for the PCRs was obtained as described above. All primers can be found in
492 ***Supplementary table 3***.

493 **Phenotypic CRISPR-Cas9 functionality assay**

494 To check for the presence of dysfunctional CRISPR-Cas9 activity in cefotaxime-resistant
495 escapers from isolates Ecp1-I and Ecp1-II that showed expected lengths of csgc amplicons and,
496 in cefotaxime-sensitive escapers, a phenotypic CRISPR-Cas9 functionality assay was performed.
497 For this assay, liquid conjugations were performed with donors harbouring either plasmid
498 pCTX15, which we engineered to carry $bla_{CTX\text{-}M\text{-}15}$, or plasmid pCTRL, which we engineered to carry
499 a mutated version of $bla_{CTX\text{-}M\text{-}15}$ that allows escape from CRISPR-Cas9 targeting through a silent
500 point mutation of the PAM sequence. Specific details about plasmid engineering and the assay
501 can be found in ***Supplementary method 1*** and ***2***.

502 **Phenotypic β-galactosidase assay**

503 To characterize the IS*Ecp1* $bla_{CTX\text{-}M\text{-}15}$ deletions found in cefotaxime-sensitive escapers from
504 isolates Ecp1-I and Ecp1-II, a phenotypic β-galactosidase assay was performed that makes use
505 of the proximity of $bla_{CTX\text{-}M\text{-}15}$ to the *lacZ* gene. Individual escapers were plated onto 0.2 µg mL^{-1} X-
506 Gal LB-agar plates. Colonies were screened for white (β-galactosidase / *lacZ*-negative) or blue (β-
507 galactosidase / *lacZ*-positive) phenotypes. Cefotaxime-resistant escapers, transconjugants from
508 the pKJK5::csgc[NT] control and the ancestral isolates were used as positive controls.

509 **Sequencing**

510 Whole genome sequencing was performed to obtain genomic details of the four *E. coli* ST131
511 ancestral isolates and several escapers from the CRISPR-Cas9 treatment. For the ancestral
512 isolates, DNA extraction was performed from LB + CTX 3 µg mL^{-1} ON cultures using FastDNA Spin
513 Kit (MP Biomedicals). The extracted DNA was treated with 2 µL of RNAseA 20 mg mL^{-1} for 10
514 minutes at 37 °C and purified with SPRISelect beads (Beckman Coulter). Sequencing libraries
515 were prepared with 2 µg of purified DNA using the ONT Ligation Sequencing Kit (Oxford Nanopore
516 Technologies) and long-read sequencing was performed using PromethION (Exeter Sequencing
517 Facility). Genomes were assembled using *Unicycler* (version 0.5.0) (85), with automated
518 annotations generated using *RASTtk* (86). Short-read WGS (MicrobesNG, Birmingham) was
519 performed for one β-galactosidase-positive and one β-galactosidase-negative cefotaxime-
520 sensitive escaper from isolates Ecp1-I and Ecp1-II. Similarly, short-read WGS (MicrobesNG,
521 Birmingham) was also performed for escaper 5.10 from isolate Ecp1-II. Hybrid WGS
522 (MicrobesNG, Birmingham) was performed for ten cefotaxime-sensitive escapers from isolate
523 26-II (two per each filter mating replicate) and for one transconjugant from the pKJK5::csgc[NT]
524 control. Genome assembly was performed using *Flye* (87) and the respective deletions were
525 characterized. Benchling was used for DNA visualization (88).

526 **Data analysis**

527 Data processing, visualisation and statistical analyses were performed in R version 4.4.2 using R
528 studio 2023.9.1.494 (89). Statistical modelling was performed using package *lme4* (version 1.1-
529 37) (90). Data processing and plotting were performed using packages *tidyverse* (version 2.0.0)
530 (91), *ggplot2* (version 3.5.1) (92), *gggenes* (version 0.5.1) (93), *patchwork* (version 1.3.1) (94) and
531 *grid* (version 4.4.2) (89). Significance of fixed effects was determined through comparing nested
532 models using chi-squared tests ($\alpha = 0.05$), beginning with a global model that included all
533 biologically relevant fixed effects and interaction terms. Interaction term statistical significance
534 was always tested first, and where interactions were statistically significant, all constituent fixed
535 effects were retained in the model. R package *DHARMa* (version 0.4.6) (95) was used to diagnose
536 potential model issues. Specifically, we checked if residuals deviation were deviated from the
537 expected distribution, if the model had over or under dispersion, if the datasets contained highly
538 influential outliers, and if the residuals were heteroscedastic. Post-hoc analyses were performed
539 using *emmeans* (version 1.10.2) (96).

540 Conjugation efficiency of CRISPR-Cas9 and the cefotaxime-resistant and cefotaxime-sensitive
541 escape frequencies were modelled using binomial family generalised linear models (GLMs) and
542 a logit link function, with the number of colonies counted for the recipients and transconjugants
543 as the weights value. Due to large differences in the count of transconjugants between
544 treatments, concentrations of recipients and transconjugants (CFU/mL) were logarithmically
545 transformed (when the dataset included zeros, log10+1 was used).

546 Our global model of conjugation efficiency of CRISPR-Cas9 included the predictor variables
547 plasmid identity, isolate identity, and an interaction between plasmid and isolate identity. For the
548 cefotaxime-resistant and cefotaxime-sensitive escape frequency analyses we modelled the
549 predictor variable genetic context of the $bla_{\text{CTX-M-15}}$. For the cefotaxime-sensitive escape
550 frequencies, model validation revealed slight deviation in the first quartile of the residuals *vs*
551 predicted plot. However, this model remained the most appropriate, and the large observed
552 effect sizes mean it is improbable we are drawing erroneous conclusions from this analysis. For
553 the cefotaxime-resistant escape frequencies, model validation revealed some influential outliers
554 (replicates with no escapers) and model optimization was performed removing outliers.

555 For the phenotypic CRISPR-Cas9 functionality assay in *E. coli* K-12 MG1655 carrying either
556 pKJK5::csgc[NT] or pKJK5::csgc[$bla_{\text{CTX-M-15}}$] the relative conjugation efficiencies (pCTRL/pCTX15)
557 were modelled using a Gamma family GLM with a log link function and with CRISPR-Cas9
558 plasmid as a predictor variable. For the phenotypic CRISPR-Cas9 functionality assay with

559 escapers, the data were individually modelled for each isolate. For both datasets, pCTRL/pCTX15
560 was modelled using a Gamma family GLM with a log link function, with cefotaxime phenotype as
561 a predictor variable. Model validation revealed some heteroscedasticity for isolate Ecp1-II, which
562 could be attributed to the presence of few cefotaxime-sensitive escapers with dysfunctional
563 CRISPR-Cas9 systems. Nevertheless, the Gamma GLM remained the most appropriate for our
564 data.

565 **DATA AVAILABILITY**

566 The genome of the *E. coli* ST131 isolates (Ecp1-I, Ecp1-II, 26-I, 26-II) were deposited in
567 PRJNA1281408. The assembled genomes of escapers with $bla_{\text{CTX-M-15}}$ deletions from isolates
568 Ecp1-I, Ecp1-II and 26-II and for escaper 5.10 Ecp1-II can be found in __*to be determined*__. The
569 data analysis can be found in GitHub __*to be determined*__. All the raw data and the full escape
570 characterization can be found in the raw data excel file in __*to be determined*__. Additional
571 experimental details, methods, tables and figures can be found in the online version of this
572 article.

573 **ACKNOWLEDGEMENTS AND FUNDING**

574 S.V.H. gratefully acknowledges funding from the Biotechnology and Biological Sciences Research
575 council (BBSRC; BB/R010781/1), the Lister Institute for Preventative Medicine, and the Joint
576 Programme Initiative AntiMicrobial Resistance (JPI-AMR) 'Harissa' call (MISTAR;
577 MR/W031191/1)). D.S was supported in part by grant MR/N0137941/1 for the GW4 BIOMED MRC
578 DTP, awarded to the Universities of Bath, Bristol, Cardiff and Exeter from the Medical Research
579 Council (MRC)/UKRI. Genome sequencing of the ST131 isolates was supported by funding from
580 the Natural Environment Research Council awarded to AFCL (award number NE/R013748/1) and
581 utilised equipment funded by the UK Medical Research Council (MRC) Clinical Research
582 Infrastructure Initiative (award number MR/M008924/1). For the purpose of open access, the
583 author has applied a 'Creative Commons Attribution (CC BY) licence to any Author Accepted
584 Manuscript version arising from this submission.

585 **Bibliography**

586 1. Naghavi M, Vollset SE, Ikuta KS, Swetschinski LR, Gray AP, Wool EE, et al. Global burden of
587 bacterial antimicrobial resistance 1990–2021: a systematic analysis with forecasts to
588 2050. The Lancet. 2024 Sep 28;404(10459):1199–226.

589 2. Dadgostar P. Antimicrobial Resistance: Implications and Costs. Infect Drug Resist. 2019
590 Dec 20;Volume 12:3903–10.

591 3. Haney EF, Hancock REW. Addressing Antibiotic Failure—Beyond Genetically Encoded
592 Antimicrobial Resistance. Front Drug Discov. 2022;2:892975.

593 4. Murray CJ, Ikuta KS, Sharara F, Swetschinski L, Robles Aguilar G, Gray A, et al. Global
594 burden of bacterial antimicrobial resistance in 2019: a systematic analysis. Lancet.
595 2022;399(10325):629–55.

596 5. World Health Organization. Prioritization of pathogens to guide discovery, research and
597 development of new antibiotics for drug-resistant bacterial infections, including
598 tuberculosis. 2017.

599 6. Poolman JT, Wacker M. Extraintestinal Pathogenic Escherichia coli, a Common Human
600 Pathogen: Challenges for Vaccine Development and Progress in the Field. J Infect Dis.
601 2016 Jan 1;213(1):6–13.

602 7. Daga AP, Koga VL, Soncini JGM, de Matos CM, Perugini MRE, Pelisson M, et al. Escherichia
603 coli Bloodstream Infections in Patients at a University Hospital: Virulence Factors and
604 Clinical Characteristics. Front Cell Infect Microbiol. 2019 Jun 6;9:191.

605 8. Manges AR, Geum HM, Guo A, Edens TJ, Fibke CD, Pitout JDD. Global Extraintestinal
606 Pathogenic Escherichia coli (ExPEC) Lineages. Clin Microbiol Rev. 2019 Jun
607 12;32(3):e00135-18.

608 9. Rogers BA, Sidjabat HE, Paterson DL. Escherichia coli O25b-ST131: a pandemic,
609 multiresistant, community-associated strain. J Antimicrob Chemother. 2011 Jan;66(1):1–
610 14.

611 10. Johnson JR, Johnston B, Clabots C, Kuskowski MA, Castanheira M. Escherichia coli
612 sequence type ST131 as the major cause of serious multidrug-resistant E. coli infections
613 in the United States. Clin Infect Dis. 2010 Aug 1;51(3):286–94.

614 11. Pitout JDD, Finn TJ. The evolutionary puzzle of Escherichia coli ST131. Infect Genet Evol.
615 2020 Jul;81:104265.

616 12. Cantón R, Coque TM. The CTX-M beta-lactamase pandemic. Curr Opin Microbiol. 2006
617 Oct;9(5):466–75.

618 13. Nicolas-Chanoine MH, Bertrand X, Madec JY. Escherichia coli ST131, an intriguing clonal
619 group. Clin Microbiol Rev. 2014 Jul;27(3):543–74.

620 14. Cantón R, González-Alba JM, Galán JC. CTX-M Enzymes: Origin and Diffusion. Front
621 Microbiol. 2012 Apr 2;3:110.

622 15. Rossolini GM, D'Andrea MM, Mugnaioli C. The spread of CTX-M-type extended-spectrum
623 beta-lactamases. Clin Microbiol Infect. 2008 Jan 1;14(Suppl 1):33–41.

16. Siguier P, Gourbeyre E, Chandler M. Bacterial insertion sequences: their genomic impact and diversity. FEMS Microbiol Rev. 2014 Sep;38(5):865–91.

17. Zhao WH, Hu ZQ. Epidemiology and genetics of CTX-M extended-spectrum β-lactamases in Gram-negative bacteria. Crit Rev Microbiol. 2013 Feb;39(1):79–101.

18. Partridge SR, Kwong SM, Firth N, Jensen SO. Mobile Genetic Elements Associated with Antimicrobial Resistance. Clin Microbiol Rev. 2018 Aug 1;31(4):e00088-17.

19. Mahillon J, Chandler M. Insertion sequences. Microbiol Mol Biol Rev. 1998 Sep;62(3):725–74.

20. Pitout JDD, Chen L. The Significance of Epidemic Plasmids in the Success of Multidrug-Resistant Drug Pandemic Extraintestinal Pathogenic Escherichia coli. Infect Dis Ther. 2023 Apr;12(4):1029–41.

21. Woodford N, Carattoli A, Karisik E, Underwood A, Ellington MJ, Livermore DM. Complete nucleotide sequences of plasmids pEK204, pEK499, and pEK516, encoding CTX-M enzymes in three major Escherichia coli lineages from the United Kingdom, all belonging to the international O25:H4-ST131 clone. Antimicrob Agents Chemother. 2009 Oct;53(10):4472–82.

22. Pajand O, Rahimi H, Darabi N, Roudi S, Ghassemi K, Aarestrup FM, et al. Arrangements of Mobile Genetic Elements among Virotype E Subpopulation of Escherichia coli Sequence Type 131 Strains with High Antimicrobial Resistance and Virulence Gene Content. mSphere. 2021 Aug 25;6(4):e0055021.

23. Varani A, He S, Siguier P, Ross K, Chandler M. The IS6 family, a clinically important group of insertion sequences including IS26. Mob DNA. 2021 Mar;23;12(1):11.

24. Harmer CJ, Hall RM. IS26 and the IS26 family: versatile resistance gene movers and genome reorganizers. Microbiol Mol Biol Rev. 2024 Jun 27;88(2):e0011922.

25. Can F, Azap OK, Seref C, Ispir P, Arslan H, Ergonul O. Emerging Escherichia coli O25b/ST131 clone predicts treatment failure in urinary tract infections. Clin Infect Dis. 2015 Feb 15;60(4):523–7.

26. Syre H, Hetland MAK, Bernhoff E, Bollestad M, Grude N, Simonsen GS, et al. Microbial risk factors for treatment failure of pivmecillinam in community-acquired urinary tract infections caused by ESBL-producing Escherichia coli. APMIS. 2020 Mar;128(3):232–41.

27. Pursey E, Sünderhauf D, Gaze WH, Westra ER, van Houte S. CRISPR-Cas antimicrobials: Challenges and future prospects. PLoS Pathog. 2018 Jun 1;14(6):e1006990.

28. Mayorga-Ramos A, Zúñiga-Miranda J, Carrera-Pacheco SE, Barba-Ostria C, Guamán LP. CRISPR-Cas-Based Antimicrobials: Design, Challenges, and Bacterial Mechanisms of Resistance. ACS Infect Dis. 2023 Jul 14;9(7):1283–302.

29. Jinek M, Chylinski K, Fonfara I, Hauer M, Doudna JA, Charpentier E. A programmable dual-RNA-guided DNA endonuclease in adaptive bacterial immunity. Science (1979). 2012 Aug 17;337(6096):816–21.

30. Jiang F, Doudna JA. CRISPR-Cas9 Structures and Mechanisms. Annu Rev Biophys. 2017 May 22;46:505–29.

664 31. Xue C, Greene EC. DNA Repair Pathway Choices in CRISPR-Cas9-Mediated Genome
665 Editing. Trends Genet. 2021 Jul;37(7):639–56.

666 32. Citorik RJ, Mimee M, Lu TK. Sequence-specific antimicrobials using efficiently delivered
667 RNA-guided nucleases. Nat Biotechnol. 2014 Nov;32(11):1141–5.

668 33. Cui L, Bikard D. Consequences of Cas9 cleavage in the chromosome of Escherichia coli.
669 Nucleic Acids Res. 2016 May 19;44(9):4243–51.

670 34. Bikard D, Euler CW, Jiang W, Nussenzweig PM, Goldberg GW, Duportet X, et al. Exploiting
671 CRISPR-Cas nucleases to produce sequence-specific antimicrobials. Nat Biotechnol.
672 2014 Nov;32(11):1146–50.

673 35. Uribe R V., Rathmer C, Jahn LJ, Ellabaan MMH, Li SS, Sommer MOA. Bacterial resistance
674 to CRISPR-Cas antimicrobials. Sci Rep. 2021 Dec 1;11(1):17267.

675 36. Reuter A, Hilpert C, Dedieu-Berne A, Lematre S, Gueguen E, Launay G, et al. Targeted-
676 antibacterial-plasmids (TAPs) combining conjugation and CRISPR/Cas systems achieve
677 strain-specific antibacterial activity. Nucleic Acids Res. 2021 Apr 6;49(6):3584–98.

678 37. Sünderhauf D, Klümper U, Pursey E, Westra ER, Gaze WH, van Houte S. Removal of AMR
679 plasmids using a mobile, broad host-range CRISPR-Cas9 delivery tool. Microbiology
680 (Reading). 2023 May;169(5):001334.

681 38. Leonard AFC, Zhang L, Balfour AJ, Garside R, Hawkey PM, Murray AK, et al. Exposure to and
682 colonisation by antibiotic-resistant E. coli in UK coastal water users: Environmental
683 surveillance, exposure assessment, and epidemiological study (Beach Bum Survey).
684 Environ Int. 2018 May;114:326–33.

685 39. Paterson DL, Bonomo RA. Extended-Spectrum β-Lactamases: a Clinical Update. Clin
686 Microbiol Rev. 2005 Oct;18(4):657–86.

687 40. Jinek M, Jiang F, Taylor DW, Sternberg SH, Kaya E, Ma E, et al. Structures of Cas9
688 Endonucleases Reveal RNA-Mediated Conformational Activation. Science (1979). 2014
689 Mar 14;343(6176):1247997–1247997.

690 41. Sihra N, Goodman A, Zakri R, Sahai A, Malde S. Nonantibiotic prevention and management
691 of recurrent urinary tract infection. Nat Rev Urol. 2018 Dec;15(12):750–76.

692 42. Durrani B, Mohammad A, Ljubetic BM, Dobberfuhl AD. The Potential Role of Persister Cells
693 in Urinary Tract Infections. Curr Urol Rep. 2023 Nov;24(11):541–51.

694 43. Reid G, Bruce AW. Probiotics to prevent urinary tract infections: the rationale and
695 evidence. World J Urol. 2006 Feb;24(1):28–32.

696 44. Gupta V, Nag D, Garg P. Recurrent Urinary Tract Infections in Women: How Promising is the
697 Use of Probiotics? Indian J Med Microbiol. 2017 Jul 1;35(3):347–54.

698 45. Jiang W, Bikard D, Cox D, Zhang F, Marraffini LA. RNA-guided editing of bacterial genomes
699 using CRISPR-Cas systems. Nat Biotechnol. 2013 Jan 29;31(3):233–9.

700 46. Neil K, Allard N, Roy P, Grenier F, Menendez A, Burrus V, et al. High-efficiency delivery of
701 CRISPR-Cas9 by engineered probiotics enables precise microbiome editing. Mol Syst Biol.
702 2021 Oct;17(10):e10335.

703 47. Hamilton TA, Pellegrino GM, Therrien JA, Ham DT, Bartlett PC, Karas BJ, et al. Efficient inter-
704 species conjugative transfer of a CRISPR nuclease for targeted bacterial killing. Nat
705 Commun. 2019 Oct 4;10(1):4544.

706 48. Gomaa AA, Klumpe HE, Luo ML, Selle K, Barrangou R, Beisel CL. Programmable removal
707 of bacterial strains by use of genome- targeting CRISPR-cas systems. mBio. 2014 Jan
708 28;5(1):e00928-13.

709 49. Vercoe RB, Chang JT, Dy RL, Taylor C, Gristwood T, Clulow JS, et al. Cytotoxic
710 Chromosomal Targeting by CRISPR/Cas Systems Can Reshape Bacterial Genomes and
711 Expel or Remodel Pathogenicity Islands. PLoS Genet. 2013 Apr;9(4):e1003454.

712 50. Li Q, Sun M, Lv L, Zuo Y, Zhang S, Zhang Y, et al. Improving the Editing Efficiency of CRISPR-
713 Cas9 by Reducing the Generation of Escapers Based on the Surviving Mechanism. ACS
714 Synth Biol. 2023 Mar 17;12(3):672–80.

715 51. Aparicio T, de Lorenzo V, Martínez-García E. CRISPR/Cas9-Based Counterselection Boosts
716 Recombineering Efficiency in Pseudomonas putida. Biotechnol J. 2018
717 May;13(5):e1700161.

718 52. Sheng Y, Wang H, Ou Y, Wu Y, Ding W, Tao M, et al. Insertion sequence transposition
719 inactivates CRISPR-Cas immunity. Nat Commun. 2023 Jul 20;14(1):4366.

720 53. Wang R, Shu X, Zhao H, Xue Q, Liu C, Wu A, et al. Associate toxin-antitoxin with CRISPR-
721 Cas to kill multidrug-resistant pathogens. Nat Commun. 2023 Apr 12;14(1):2078.

722 54. Kang YK, Kwon K, Ryu JS, Lee HN, Park C, Chung HJ. Nonviral Genome Editing Based on a
723 Polymer-Derivatized CRISPR Nanocomplex for Targeting Bacterial Pathogens and
724 Antibiotic Resistance. Bioconjug Chem. 2017 Apr 19;28(4):957–67.

725 55. Cyriaque V, Ibarra-Chávez R, Kuchina A, Seelig G, Nesme J, Madsen JS. Single-cell RNA
726 sequencing reveals plasmid constrains bacterial population heterogeneity and identifies
727 a non-conjugating subpopulation. Nat Commun. 2024;15:5853.

728 56. Moreb EA, Hoover B, Yaseen A, Valyasevi N, Roecker Z, Menacho-Melgar R, et al. Managing
729 the SOS Response for Enhanced CRISPR-Cas-Based Recombineering in E. coli through
730 Transient Inhibition of Host RecA Activity. ACS Synth Biol. 2017 Dec 15;6(12):2209–18.

731 57. Vialetto E, Miele S, Goren MG, Yu J, Yu Y, Collias D, et al. Systematic interrogation of CRISPR
732 antimicrobials in Klebsiella pneumoniae reveals nuclease-, guide- and strain-dependent
733 features influencing antimicrobial activity. Nucleic Acids Res. 2024 Jun 10;52(10):6079–
734 91.

735 58. Collias D, Vialetto E, Yu J, Co K, Almási É d. H, Rüttiger AS, et al. Systematically attenuating
736 DNA targeting enables CRISPR-driven editing in bacteria. Nat Commun. 2023 Feb
737 8;14(1):680.

738 59. Moreb EA, Hoover B, Yaseen A, Valyasevi N, Roecker Z, Menacho-Melgar R, et al. Managing
739 the SOS Response for Enhanced CRISPR-Cas-Based Recombineering in E. coli through
740 Transient Inhibition of Host RecA Activity. ACS Synth Biol. 2017 Dec 15;6(12):2209–18.

741 60. Harmer CJ, Hall RM. IS26-Mediated Formation of Transposons Carrying Antibiotic
742 Resistance Genes. mSphere. 2016 Apr 6;1(2):e00038-16.

743 61. Harmer CJ, Hall RM. IS26-Mediated Precise Excision of the IS26-aphA1a Translocatable
744 Unit. mBio. 2015 Dec 8;6(6):e01866-15.

745 62. Aihara M, Gotoh Y, Shirahama S, Matsushima Y, Uchiumi T, Kang D, et al. Generation and
746 maintenance of the circularized multimeric IS26-associated translocatable unit encoding
747 multidrug resistance. Commun Biol. 2024;7:597.

748 63. Harmer CJ, Moran RA, Hall RM. Movement of IS26-associated antibiotic resistance genes
749 occurs via a translocatable unit that includes a single IS26 and preferentially inserts
750 adjacent to another IS26. mBio. 2014 Oct 7;5(5):e01801-14.

751 64. Harmer CJ, Moran RA, Hall RM. Movement of IS26-Associated Antibiotic Resistance Genes
752 Occurs via a Translocatable Unit That Includes a Single IS26 and Preferentially Inserts
753 Adjacent to Another IS26. mBio. 2014 Oct 7;5(5).

754 65. Wang P, Du X, Zhao Y, Wang W, Cai T, Tang K, et al. Combining CRISPR/Cas9 and natural
755 excision for the precise and complete removal of mobile genetic elements in bacteria.
756 Appl Environ Microbiol. 2024 Apr 1;90(4):e0009524.

757 66. Raeside C, Gaffé J, Deatherage DE, Tenaillon O, Briska AM, Ptashkin RN, et al. Large
758 chromosomal rearrangements during a long-term evolution experiment with Escherichia
759 coli. mBio. 2014 Sep 9;5(5):e01377-14.

760 67. He S, Hickman AB, Varani AM, Siguier P, Chandler M, Dekker JP, et al. Insertion Sequence
761 IS26 Reorganizes Plasmids in Clinically Isolated Multidrug-Resistant Bacteria by
762 Replicative Transposition. mBio. 2015 Jun 9;6(3):e00762.

763 68. Poirel L, Decousser JW, Nordmann P. Insertion Sequence ISEcp1B Is Involved in Expression
764 and Mobilization of a blaCTX-M β-Lactamase Gene. Antimicrob Agents Chemother. 2003
765 Sep;47(9):2938–45.

766 69. Zong Z, Partridge SR, Iredell JR. ISEcp1-Mediated Transposition and Homologous
767 Recombination Can Explain the Context of blaCTX-M-62 Linked to qnrB2. Antimicrob
768 Agents Chemother. 2010 Jul;54(7):3039–42.

769 70. Poirel L, Lartigue MF, Decousser JW, Nordmann P. ISEcp1B-Mediated Transposition of
770 blaCTX-M in Escherichia coli. Antimicrob Agents Chemother. 2005 Jan;49(1):447–50.

771 71. Wachino JI, Yamane K, Kimura K, Shibata N, Suzuki S, Ike Y, et al. Mode of Transposition
772 and Expression of 16S rRNA Methyltransferase Gene rmtC Accompanied by ISEcp1.
773 Antimicrob Agents Chemother. 2006 Sep;50(9):3212–5.

774 72. Qi LS, Larson MH, Gilbert LA, Doudna JA, Weissman JS, Arkin AP, et al. Repurposing
775 CRISPR as an RNA-Guided Platform for Sequence-Specific Control of Gene Expression.
776 Cell. 2013 Feb 28;152(5):1173–83.

777 73. Selle K, Klaenhammer TR, Barrangou R. CRISPR-based screening of genomic island
778 excision events in bacteria. Proc Natl Acad Sci U S A. 2015 Jun 30;112(26):8076–81.

779 74. Guan J, Wang W, Sun B. Chromosomal Targeting by the Type III-A CRISPR-Cas System Can
780 Reshape Genomes in Staphylococcus aureus. mSphere. 2017 Nov 15;2(6):e00403-17.

75. Lam KN, Spanogiannopoulos P, Soto-Perez P, Alexander M, Nalley MJ, Bisanz JE, et al. Phage-delivered CRISPR-Cas9 for strain-specific depletion and genomic deletions in the gut microbiome. Cell Rep. 2021 Nov 2;37(5):109930.

76. Cañez C, Selle K, Goh YJ, Barrangou R. Outcomes and characterization of chromosomal self-targeting by native CRISPR-Cas systems in Streptococcus thermophilus. FEMS Microbiol Lett. 2019 May 1;366(9):fnz105.

77. Hu J, Crickard JB. All who wander are not lost: the search for homology during homologous recombination. Biochem Soc Trans. 2024 Feb 28;52(1):367–77.

78. Wang P, Du X, Zhao Y, Wang W, Cai T, Tang K, et al. Combining CRISPR/Cas9 and natural excision for the precise and complete removal of mobile genetic elements in bacteria. Appl Environ Microbiol. 2024 Apr 17;90(4):e0009524.

79. Kocsis B, Gulyás D, Szabó D. Emergence and Dissemination of Extraintestinal Pathogenic High-Risk International Clones of Escherichia coli. Life (Basel). 2022 Dec 10;12(12):2077.

80. Martínez-García E, Aparicio T, de Lorenzo V, Nikel PI. New transposon tools tailored for metabolic engineering of Gram-negative microbial cell factories. Front Bioeng Biotechnol. 2014 Oct 28;2:46.

81. Klümper U, Riber L, Dechesne A, Sannazzarro A, Hansen LH, Sørensen SJ, et al. Broad host range plasmids can invade an unexpectedly diverse fraction of a soil bacterial community. ISME J. 2015;9(4):934–45.

82. Forde BM, Ben Zakour NL, Stanton-Cook M, Phan MD, Totsika M, Peters KM, et al. The Complete Genome Sequence of Escherichia coli EC958: A High Quality Reference Sequence for the Globally Disseminated Multidrug Resistant E. coli O25b:H4-ST131 Clone. PLoS One. 2014 Aug 15;9(8):e104400.

83. Concordet JP, Haeussler M. CRISPOR: intuitive guide selection for CRISPR/Cas9 genome editing experiments and screens. Nucleic Acids Res. 2018 Jul 2;46(W1):W242–5.

84. Bae S, Park J, Kim JS. Cas-OFFinder: a fast and versatile algorithm that searches for potential off-target sites of Cas9 RNA-guided endonucleases. Bioinformatics. 2014 May 15;30(10):1473–5.

85. Wick RR, Judd LM, Gorrie CL, Holt KE. Unicycler: Resolving bacterial genome assemblies from short and long sequencing reads. PLoS Comput Biol. 2017 Jun 1;13(6):e1005595.

86. Brettin T, Davis JJ, Disz T, Edwards RA, Gerdes S, Olsen GJ, et al. RASTtk: A modular and extensible implementation of the RAST algorithm for building custom annotation pipelines and annotating batches of genomes. Sci Rep. 2015 Feb 10;5:8365.

87. Kolmogorov M, Yuan J, Lin Y, Pevzner PA. Assembly of long, error-prone reads using repeat graphs. Nat Biotechnol. 2019 May;37(5):540–6.

88. [Biology Software]. Benchling [Internet]. 2024. Available from: https://benchling.com

89. Posit team. RStudio: Integrated Development Environment for R [Internet]. Boston, MA: Posit Software, PBC; 2023. Available from: http://www.posit.co/

90. Bates D, Mächler M, Bolker BM, Walker SC. Fitting Linear Mixed-Effects Models Using lme4. J Stat Softw [Internet]. 2015 Oct 7;67(1):1–48. Available from: https://www.jstatsoft.org/article/view/v067i01

91. Wickham H, Averick M, Bryan J, Chang W, D' L, Mcgowan A, et al. Welcome to the Tidyverse. J Open Source Softw [Internet]. 2019 Nov 21;4(43):1686. Available from: https://joss.theoj.org/papers/10.21105/joss.01686

92. Hadley Wickham. ggplot2: Elegant Graphics for Data Analysis [Internet]. Springer-Verlag New York; 2016. Available from: https://ggplot2.tidyverse.org

93. David Wilkins. gggenes: Draw Gene Arrow Maps in "ggplot2" [Internet]. 2020. Available from: https://CRAN.R-project.org/package=gggenes

94. Thomas Lin Pedersen. patchwork: The Composer of Plots [Internet]. 2025. Available from: https://patchwork.data-imaginist.com

95. Hartig F. DHARMa: Residual Diagnostics for Hierarchical (Multi-Level / Mixed) Regression Models. CRAN: Contributed Packages. 2016.

96. Lenth R V. emmeans: Estimated Marginal Means, aka Least-Squares Means. CRAN: Contributed Packages. 2017.